NANO LETTERS

Letter

Cite This: Nano Lett. 2019, 19, 5746−5753

pubs.acs.org/NanoLett

Real-Time Assembly of Viruslike Nucleocapsids Elucidated at the Single-Particle Level

Margherita Marchetti,[†,‡] Douwe Kamsma,[†] Ernesto Cazares Vargas,[§] Armando Hernandez García,[§] Paul van der Schoot,[∥,#] Renko de Vries,[⊥] Gijs J. L. Wuite,[*,†,×] and Wouter H. Roos[*,‡,×]

[†]Department of Physics and Astronomy and LaserLaB Amsterdam, Vrije Universiteit Amsterdam, 1081 HV Amsterdam, The Netherlands

[‡]Moleculaire Biofysica, Zernike Instituut, Rijksuniversiteit Groningen, 9712 CP Groningen, The Netherlands

[§]Institute of Chemistry, Department of Chemistry of Biomacromolecules, National Autonomous University of Mexico, 04510 Mexico City, Mexico

[∥]Institute for Theoretical Physics, Utrecht University, 3512 JE Utrecht, The Netherlands

[#]Department of Applied Physics, Eindhoven University of Technology, 5612 AZ Eindhoven, The Netherlands

[⊥]Laboratory of Physical Chemistry and Colloid Science, Wageningen University, 6708 PB Wageningen, The Netherlands

Supporting Information

ABSTRACT: While the structure of a multitude of viral particles has been resolved to atomistic detail, their assembly pathways remain largely elusive. Key unresolved issues are particle nucleation, particle growth, and the mode of genome compaction. These issues are difficult to address in bulk approaches and are effectively only accessible by the real-time tracking of assembly dynamics of individual particles. This we do here by studying the assembly into rod-shaped viruslike particles (VLPs) of artificial capsid polypeptides. Using fluorescence optical tweezers, we establish that small oligomers perform one-dimensional diffusion along the DNA. Larger oligomers are immobile and nucleate VLP growth. A multiplexed acoustic force spectroscopy approach reveals that DNA is compacted in regular steps, suggesting packaging via helical wrapping into a nucleocapsid. By reporting how real-time assembly tracking elucidates viral nucleation and growth principles, our work opens the door to a fundamental understanding of the complex assembly pathways of both VLPs and naturally evolved viruses.

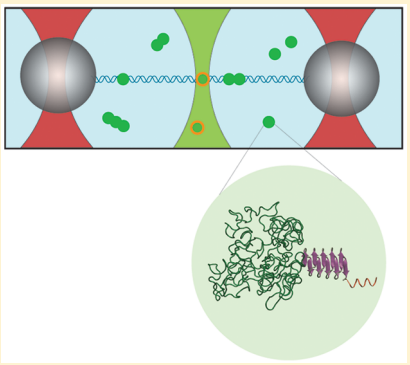

KEYWORDS: *Self-assembly, artificial virus, physical virology, biophysics, optical tweezers, acoustic force spectroscopy*

The structure of viral particles is typically highly regular and remarkably stable.[1] A number of viruses have been reconstituted *in vitro*, suggesting that quite generic physical driving forces determine their assembly pathways. This motivated trials to replace viral genomes with other cargo, allowing viruses to be employed, *e.g.*, as drug delivery platforms.[2−4] Many bulk experimental studies[5−8] as well as modeling and computer simulation approaches[9−11] have been performed to elucidate the *in vitro* assembly pathways of viral particles. An important conclusion is that the multiplicity of assembly pathways in the experiments obscures interpretation of the findings.[12] Central questions yet to be answered include the nature of the critical nuclei required for productive viral particle formation as well as the nature and dynamics of nucleic acid condensation during particle formation.[13−15] In order to discriminate between different pathways and to identify assembly intermediates, real-time assembly of viral particles should be probed at the single-particle level.

Single molecule techniques such as electron microscopy and atomic force microscopy (AFM) provide for high-resolution images of viruses but typically yield images with only limited information on dynamic assembly pathways.[16,17] High-resolution AFM imaging and electron microscopy have recently provided access to information on transient capsid intermediates from which kinetic assembly parameters can be estimated.[18] In addition, new approaches, such as resistive-pulse sensing in nanofluidic devices, probe late-state intermediates during viral assembly.[19] Here we go beyond these recent studies by using combined confocal fluorescence and optical tweezing to identify the nature of critical nuclei in capsid formation. In addition, we use acoustic force spectroscopy to probe in real-time not only the dynamics and nature of particle growth but also nucleic acid condensation during the formation of single, rod-shaped nucleocapsid particles.

We do this for a previously *de novo* designed artificial capsid polypeptide bearing a stretch of lysines,[20] which interacts through electrostatic interactions with the phosphates of single

Received: June 11, 2019
Revised: July 24, 2019
Published: August 1, 2019

or double-stranded DNA templates to coassemble into rod-shaped viruslike particles (VLPs). This polypeptide was designed to mimic the essential features of the *in vitro* assembly of Tobacco Mosaic Virus particles, viz. obligate coassembly with a linear nucleic acid template, with growth proceeding from a single nucleus. Indeed, the time evolution of the particle size distributions of both TMV and the VLPs can be accurately fitted to the same kinetic model, yielding similar energies for particle nucleation and particle growth.[9,20,21] The rod-shaped VLPs consist of a single DNA molecule coated with multiple copies of the artificial capsid polypeptide. The latter we refer to as C−S_{10}−B, with each of its three blocks encoding a specific physicochemical functionality, mimicking corresponding functionalities of viral capsid proteins (Figure 1A).

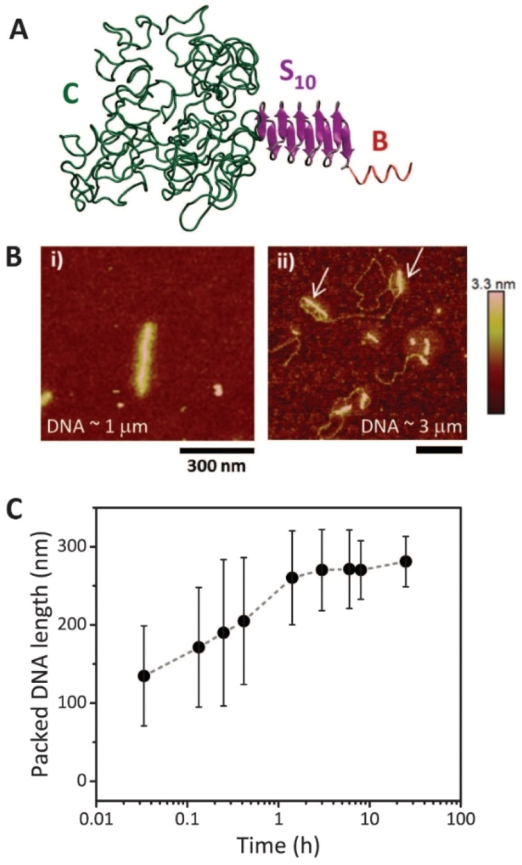

Figure 1. Artificial capsid polypeptide under investigation and the resulting formation of rod-shaped particles. (A) Schematic of the triblocks polypeptide C−S_{10}−B. Each block is highlighted by a different color and its specific function, related to its physiochemical properties, as described in the methods. (B) Particle formation on DNA molecules of different lengths was probed with AFM imaging in the air. On DNA of ∼1 μm contour length, mainly single particles form in which the DNA is compacted 1/3 of its original length (panel i). When a 3-fold longer DNA is employed (∼3 μm contour length), 2−4 nucleation points are observed in the early stages of particles assembly (panel ii). The white arrows point at two different nucleation sites that are formed on the same DNA molecule. (C) Quantification from AFM images of the "slow" kinetics of particle formation on a 2.5 kbp DNA, being packed to 1/3 of its original length, as also previously shown.[20] Error bars are standard deviations and for each time point ∼100 particles were analyzed.

We here use these simple model capsid polypeptides to address key issues regarding capsid assembly pathways not only in real-time but also at the single-particle level. We study the nature of the critical nuclei for productive capsid formation, the dynamics of particle growth, and the dynamics and nature of nucleic acid condensation during capsid formation. Our study on this simple model system paves the way for detailed real-time *in vitro* studies of the assembly of naturally evolved viruses at the single-particle level.

Results. *Real-Time Observation of Nucleation on Long DNA.* First we use atomic force microscopy (AFM) imaging to recapitulate basic properties of encapsulation of linear DNA by the artificial capsid polypeptides.[17] Upon mixing the capsid polypeptides with double-stranded DNA, rod-shaped particles are formed, confirming earlier findings[20] (Figure 1B). The kinetics of particle formation can be quantified by analyzing the length of packaged DNA as a function of time (Figure 1C). DNA with a contour length <1 μm typically displays one or two nucleation sites, while longer DNA with a contour length >1 μm often shows more than two nucleation sites (Figure 1B). The relative frequency of the number of nucleation points and the resulting branches in the self-assembled particle were quantified for a 2.5 kbp-long DNA (contour length of ≈850 nm) (Fig. S1). Next to imaging in air, we additionally performed AFM imaging in aqueous solution. This yielded an average diameter of the VLPs of 9 nm, a value that matches the expected lateral dimensions of the VLP (Fig. S1).

Next we turn to investigating the assembly of single viruslike particles in real-time, first considering the nucleation of artificial capsids on their DNA templates. Specifically, we wish to elucidate the nature of the critical nuclei required for productive capsid growth. For this, we combine confocal fluorescence microscopy and optical tweezing.[22] A long DNA molecule (λ-phage DNA, contour length ≈16.5 μm) is attached at both ends to a microsphere ("bead"), and both beads are trapped using a double optical tweezers setup. Simultaneous confocal scanning laser microscopy allows for real-time probing of the local binding of fluorescently labeled artificial capsid polypeptides on the DNA[23] (Figure 2A). Because the DNA in this assay is long, multiple nuclei are expected to form (Fig. S1), making this technique particularly well suited to zoom in on VLP nucleation events. First, nucleation is allowed to proceed unimpeded by repeatedly keeping the DNA in a relaxed state (<1 pN) for a fixed amount of time (5 min), followed by a short period of imaging at a constant force of 5 pN (Figure 2B). We observe a shortening of the end-to-end distance as a function of time, indicating condensation of the DNA during the relaxed state phases (Figure 2B,i). We also observe an increasing number of nuclei as a function of time and a corresponding increase of the total fluorescence intensity (Figure 2B,ii). With these findings, which are supported by our AFM data, we confirm that in our dynamic assay multiple nucleation sites are indeed formed, capable of compacting the DNA in a progressive way.

In order to study the mechanical effect of polypeptide binding to the DNA, relaxed DNA was first incubated with the proteins in solution, then stretched to an end-to-end distance nearly equal to its contour length, and subsequently relaxed back to zero force while recording the retraction force (Figs. S2 and S3). We find that the apparent persistence length L_p obtained by fitting a wormlike chain model to the retraction force[24] decreases sharply as the number of bound capsid polypeptides increases (Fig. S2B). This is consistent with the

DOI: 10.1021/acs.nanolett.9b02376
Nano Lett. 2019, 19, 5746−5753

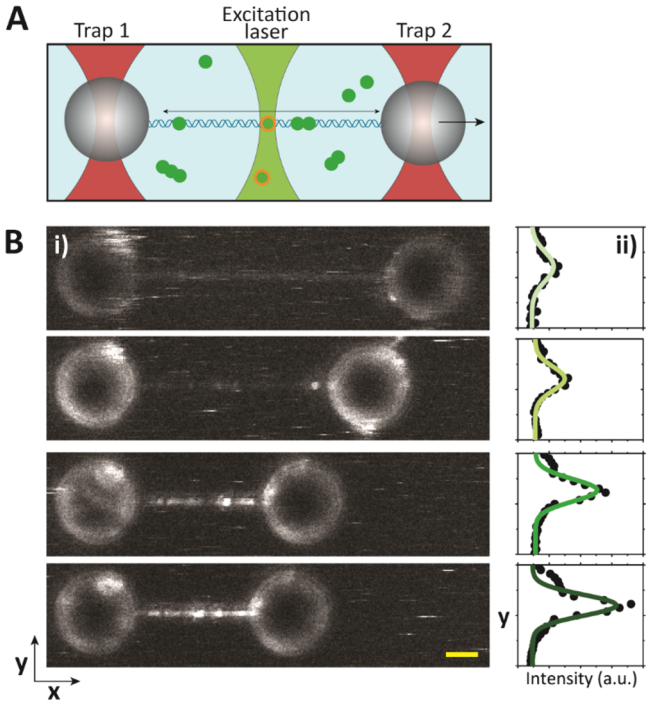

Figure 2. Optical tweezers combined with confocal fluorescence microscopy reveals protein binding and compaction. (A) Illustration of a dual trap optical tweezers combined with confocal fluoresce microscopy. Two focused lasers beams (red) trap two microspheres that are chemically attached to a DNA molecule. Proteins in solution (green dots) bind to the DNA, and their fluorescence tag lights up when the scanning laser (light green beam) illuminates them. (B) Progressive packaging of the DNA by the polypeptides. (i) Confocal fluorescence images show how DNA shortening (from top to bottom, time = 0, 5, 15, 25 min. Yellow scale bar, 2.5 μm) is accompanied by an increase in the fluorescence intensity. (ii) Plots of fluorescence intensity, which is directly related to the number of bound peptides (fluorescence images *y*-position vs integrated fluorescence intensity (a.u.) along the DNA).

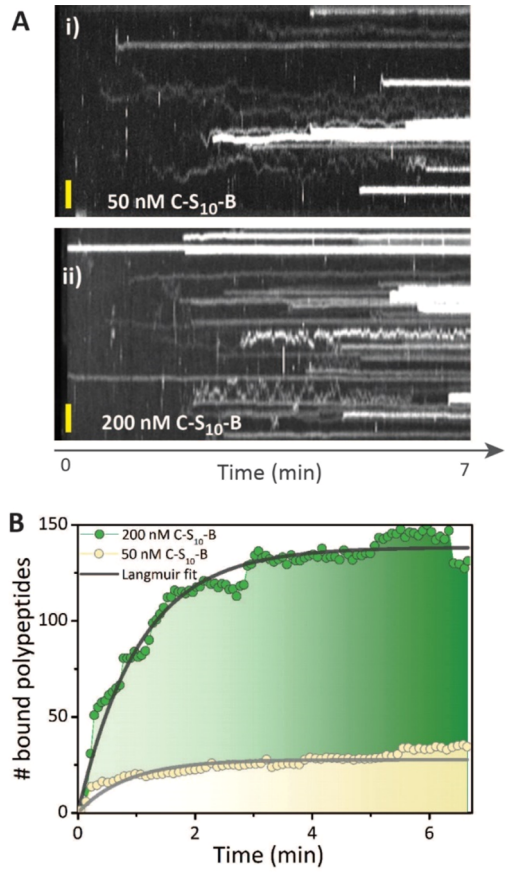

Figure 3. Real-time polypeptide binding. (A) Kymographs showing progressive peptide binding for two different C−S_{10}−B concentrations: 50 nM panel (i) and 200 nM panel (ii). The confocal scanning line-time is 30 ms, the yellow scale bar denotes 2 μm. (B) Cumulative polypeptide binding over time (data extracted from the kymograph integrated intensity over time). Average values from six kymographs at 200 nM (green dots) and five kymographs at 50 nM (yellow dots) are plotted. The data were fitted with a Langmuir adsorption model resulting in a polypeptide binding constant of $K \approx 7 \times 10^8$ M^{-1}.

occurrence of induced deformations during DNA compaction, such as kinking or bending.[25,26] Indeed, the control polypeptide C−B, lacking the central S_{10} silklike block, known to simply coat but not condense the DNA,[27] does not show the reduction of persistence lengths (Fig. S3D).

Identification of the Nature of Critical Nuclei Required for Artificial Capsid Formation. In the experiments shown in Figure 2, nucleation and growth proceeds unimpeded as the DNA is in a relaxed state for fixed times, only to be stretched for a short time for imaging purposes. This precludes the observation of capsid nucleation with high temporal resolution. Therefore, we performed experiments to quantify polypeptide binding dynamics at the single-molecule level and at millisecond time scales. We keep the DNA at a fixed end-to-end distance of 15.5 μm and continuously monitor the fluorescence along the 16.5 μm contour length long DNA in the form of kymographs (Figure 3A). For these experiments, the fluorescence intensity of one dye molecule was established to be 12.0 ± 0.5 photons (see Methods and Fig. S4), with which the absolute number of bound polypeptides can be determined.[28]

As DNA compaction progresses, high forces quickly develop that most likely decreases polypeptides binding and halts DNA condensation on the stretched DNA. Indeed, the number of bound capsid polypeptides as a function of time, shown in Figure 3B for two polypeptide concentrations, plateaus after about 5 min, at levels far below saturation (see Figure 3A). With the assumption that the stretching mainly influences the maximum number of bound polypeptides, but not the binding dynamics, these data were analyzed using a simple reversible Langmuir adsorption kinetics model[29] (Supporting Information). This resulted in an effective binding free energy of ~25 times the thermal energy, which is of the same order of magnitude as earlier estimates for VLP growth.[9,30]

The calibrated kymograph data yields distributions of the number of polypeptides involved in each binding event. From Figure 4A it can be seen that at 50 nM the most frequent cluster size is a trimer, whereas at 200 nM it is a hexamer. By tracking single traces to obtain mean-square displacements[31] of polypeptide clusters moving on the DNA over time, we extracted diffusion constants of polypeptide clusters bound to the DNA as a function of cluster size (Figure 4B). We find that small clusters slide along the DNA, while large clusters are essentially immobilized on the DNA. The mobility of clusters drops to essentially zero for pentameric and larger oligomers ($D \leq 0.1 \times 10^{-2}$ $\mu m^2/s$). The observed decrease of the

DOI: 10.1021/acs.nanolett.9b02376
Nano Lett. 2019, 19, 5746−5753

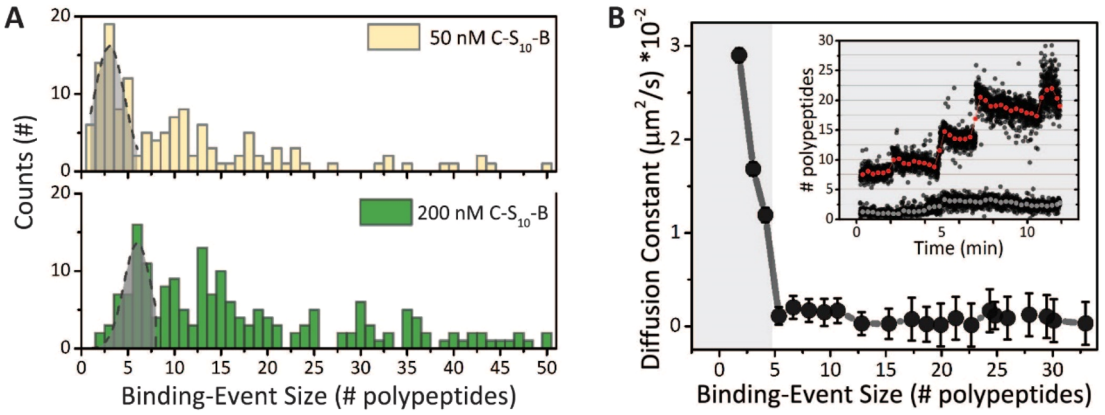

Figure 4. Polypeptide size quantification and their mobility along the DNA. (A) Quantification of single photobleaching steps allows an estimation of the number of polypeptides bound per recorded event. The binding-event size statistics produces a histogram with a broad range of binding sizes. At 50 nM, the first observed peak fits with trimer binding (Gaussian peak, 3.0 ± 0.4 polypeptides). At 200 nM, the first observed peak fits with hexamer binding (6.0 ± 0.3 polypeptides). (B) Diffusion constant D of the tracked binding events in the kymographs reveals an initial, drastic drop with increasing oligomer size, leveling off for oligomer sizes of ≥5 polypeptides (gray background area highlights the mobile events, error bars SEM). Inset: example of single binding events indicating that oligomer growth is more likely (90% traces) to take place when starting off with a large cluster (>5-mer, red curve) than with a small cluster (gray curve in the example, 10% traces).

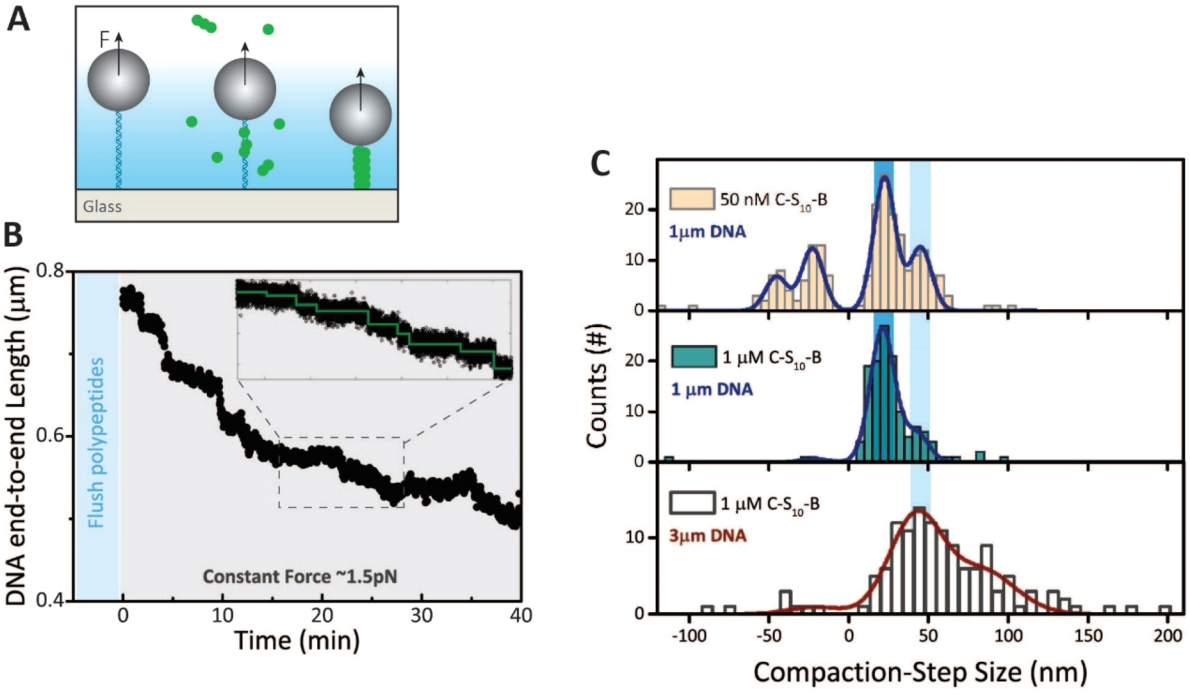

Figure 5. Acoustic force spectroscopy reveals particles compaction dynamics. (A) Illustrative image of the AFS setup. DNA tethered microspheres are pushed along an acoustically generated pressure gradient (blue/white background) that applies a long and stable low-force clamp. (B) Decrease in DNA end-to-end length over time is a measure of the DNA compaction. The light blue background indicates the flushing in of peptides into the flow-cell while a stretching force of 15 pN is applied. The gray background area indicates a constant applied force of 1.5 pN. Inset: close-up of a compaction trace with the green line of the fit showing the compaction steps found with a previously developed step finding algorithm.[33] (C) Step size statistics of compaction events at different conditions: 50 nM polypeptides−1 μm DNA (top histogram), 1 μM polypeptides−1 μm DNA (middle histogram), and 1 μM polypeptides−3 μm DNA (bottom histogram). The negative steps obtained at lower concentration (top histogram) are decompaction events, which shows a symmetrical distribution. The compaction event data are fitted with a multi-Gaussian function, where the distances from peaks-to-peak are equally spaced and used as one fit parameter.

diffusion constant with cluster size is much steeper than is expected for a simple linear scaling of the sliding friction with oligomer size (see Fig. S3C), suggesting strong interactions of the large oligomers with the DNA and likely conformational integration into growing VLPs.

Further analysis of the intensity of the polypeptide clusters reveals that those clusters that are smaller than pentamers only grow in 10% of the cases. For pentameric and larger clusters, this occurs in 90% of the cases (Figure 4B, inset). Previously, it has been shown that a minimal number of polypeptides need to simultaneously bind to the DNA in order to nucleate particle growth.[21] This should also mean that for very short DNA, covered by fewer proteins than the critical nucleus, the binding strength of the proteins should drop to lower values.

DOI: 10.1021/acs.nanolett.9b02376
Nano Lett. 2019, 19, 5746−5753

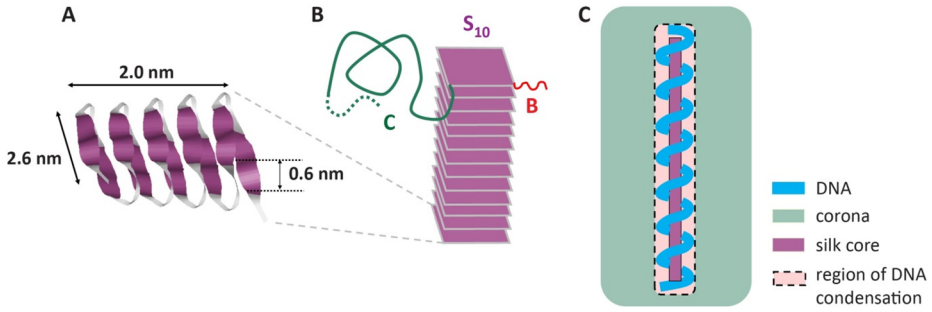

Figure 6. Conformation of condensed DNA. (A) Sheetlike beta-solenoid conformation of folded silk block S_{10} = $(GAGAGAGQ)_{10}$ with approximate dimensions, as predicted by computer simulations.[38] (B) Filamentous core of the VLPs is formed through stacking of the sheetlike folded silk blocks. (C) Region of DNA condensation extends from just outside the filamentous core up to the distance the flexible oligolysine binding blocks B = K_{12} can stretch away from the filamentous core from which they emanate, which is a few nanometers. Binding to the highly localized binding blocks may lead to different condensed conformations of the DNA such as a helical winding around the filamentous core of the VLP, as suggested by the observation of regular condensation and decondensation steps of 30 nm of DNA contour length.

Indeed, a bulk electrophoretic mobility shift assay (EMSA) confirms that binding of the artificial capsid polypeptides is strongly dependent on the length of the DNA template in the range of 10 bp to 1000 bp (Fig. S5). Taken together, our data strongly suggests that preformed oligomers bind to the DNA, and that pentamers, if bound to the DNA, should be considered as the critical nuclei for the productive formation of VLPs.

Nature and Dynamics of DNA Condensation during Capsid Growth. The combined fluorescence microscopy and optical tweezers experiments discussed previously are suboptimal for studying capsid growth. This is because (i) the many nuclei on the long DNA (Fig. S1C) make it difficult to follow growth of each of them, and (ii) growth of the nuclei cannot be followed over a sufficiently long time due to photo bleaching. Therefore, as a complementary real-time, single-particle technique, we apply acoustic force spectroscopy (AFS). AFS allows us to probe end-to-end distances for short DNA molecules tethered between a surface and a microbead (see schematic in Figure 5A) as a function of time (up to hours), for a fixed low force and with high temporal resolution (50 Hz).[32] Since the DNA used in the AFS experiment is short (2.9 kbp ≈ 1 μm), growth of viruslike particles is initiated from one or at most two nuclei (Fig. S1A,B), allowing us to follow growth in much greater detail. Data for multiple DNA strands is acquired simultaneously, leading to superior statistics.

After confirming that results for the effective persistence lengths obtained from force–extension curves obtained by optical tweezers agree with those obtained from force–extension curves obtained by AFS (Fig. S6A,B), we apply AFS to probe in detail the nature and dynamics of DNA condensation during capsid growth. The DNA condensation is observed in real-time by measuring the end-to-end distance of DNA molecules kept at fixed low force of 1.5 pN and in the presence of artificial capsid polypeptides.

Surprisingly, we find that DNA condensation into viruslike particles proceeds in a stepwise fashion (Figure 5B, inset). A multi-Gaussian distribution with equally spaced peak distances is fitted to the extracted step sizes. The short DNA (≈ 1 μm) reveals a sharp peak at a step size of 30 ± 1 nm in DNA contour length for both low (50 nM) as high (1 μM) C–S_{10}–B concentrations (Figure 5C). This shows that the most probable step size for the condensation process is concentration independent. At low polypeptide concentrations, we also find decondensation steps, recorded as negative steps. Remarkably, the most probable step sizes for condensation and decondensation appear equal, not only at low forces but also if we increase the tension in order to induce decondensation (Fig. S6C). Employing a 3-fold longer DNA (8.3 kbp ≈ 3 μm), the step-size distribution has much less pronounced peaks, which we attribute to the presence of multiple growing nuclei on the longer DNA. In this case, simultaneous steps at multiple locations cannot be deconvoluted and are detected as larger steps (Figure 5C).

Discussion. The self-assembly pathway of even relatively simple viruses, such as the tobacco mosaic virus that consists of a single-stranded RNA packaged by a large number of identical copies of coat protein, is highly complex. It is only partially understood and in fact remains the object of controversy.[9] At least in part this is due to the circumstance that capsid assembly pathways are difficult to address other than with real-time, single-particle methods. Two unresolved issues are considered in this work: the nature of the critical nuclei for productive capsid formation and the dynamics and nature of nucleic acid condensation during capsid growth. For a simple artificial capsid polypeptide model system, which mimics essential features of the assembly of the much more complicated natural tobacco mosaic virus, we have shown that powerful, real-time, single molecule techniques can be used to successfully address such issues.

For these artificial capsid polypeptides, we have shown that a broad range of preformed polypeptide oligomers can directly bind the DNA. As described by classical nucleation theory of protein capsids, a nucleus with a certain critical size has to be reached to trigger capsid formation, which seems to be true for spherical and rodlike assemblies alike.[14,21,34,35] We find that binding events of oligomers consisting of less than five polypeptides typically do not lead to particle growth. These oligomers, when bound, slide along the DNA with a mobility that rapidly decreases with increasing oligomer size. Binding events of oligomers consisting of minimally five polypeptides seem to be required for triggering nucleocapsid growth. Such oligomers, when bound to the DNA, are essentially immobile. Therefore, we conclude that pentamers bound to the DNA template may be considered to be the critical nuclei for the formation of the artificial capsids. The smaller-sized oligomers (<5) that can slide along the DNA may assist the growth process. Indeed, proteins sliding along a nucleic acid molecule

DOI: 10.1021/acs.nanolett.9b02376
Nano Lett. 2019, 19, 5746–5753

during viral assembly is theoretically shown to considerably accelerate the self-assembly of natural icosahedral viruses.[36,37]

The nature and dynamics of DNA condensation during capsid growth was successfully addressed using AFS, for it allows probing end-to-end distances of multiple short DNAs over prolonged periods of time and under a precisely controlled low force. Surprisingly, we have established that DNA condensation into the artificial capsids occurs in discrete single compaction events, with approximately 30 nm of DNA contour length being condensed in each compaction event. This characteristic length of DNA per compaction event seems to be largely independent of the protein concentration and therefore also independent of nuclei size. Also, decondensation steps at low protein concentrations show the same characteristic length, suggesting that this length of DNA must corresponds to a characteristic structure of condensed DNA in the rod-shaped artificial viral capsid.

The filamentous core of the VLP is formed by the silklike middle blocks S_{10} of the C−S_{10}−B artificial capsid polypeptide, which assemble into a stack of beta-solenoids (Figure 6A,B). Each beta-solenoid sheet has a dimension of ≈2.0 nm × 2.6 nm and a height of ≈0.6 nm, as predicted by computer simulations.[38,39] The binding blocks B and stability block C emanate from the filamentous core. From this we expect that the DNA is confined to a condensation region extending at most a few nanometers away from the filamentous core (Figure 6), since the flexible dodecalysine binding blocks B can only extend up to that distance. Such a structure is consistent with the height of the VLPs found using AFM imaging in liquid (Fig. S1C), which show an average particle height of ≈9 nm.

The question arises what conformation the DNA adopts in the condensation region close to the filamentous core of the VLPs. For DNA packed into icosahedral spaces such as in T4 and T7 bacteriophages, it has convincingly been shown that the experimentally observed spool-like DNA configuration can be explained purely in terms of nanogeometric confinement.[40−42] In other cases, binding to capsid proteins may induce nucleic acid template deformations that would not be expected on the basis of geometric confinement alone. For example, the helical arrangement of the RNA genome in TMV virus particles is dictated by their binding to the capsid proteins rather than by geometric confinement.[43] For our artificial viruslike particles, it has previously been shown that particle lengths are roughly one-third of the DNA contour length.[20] If the DNA conformation inside the artificial viruslike particles considered here is determined by geometric nanoconfinement alone, the most plausible conformation would be that of parallel double stranded DNAs with hairpin bending defects, as illustrated in Fig. S7. Such conformations minimize the bending energy of semiflexible chains in finite length tubular confinement, for tube diameters much less than the persistence length, as predicted in recent computer simulations[44] and demonstrated by the theoretical estimates of eqs S10−S12. Such conformations are also similar to the conformations adopted by DNA confined in nanochannels.[45]

However, binding of the DNA to the highly localized binding blocks that emanate from the filamentous core may induce strong DNA deformations that in turn lead to DNA conformations very different from those predicted for confinement of the DNA in a finite nanotube. Indeed, the observed 30 nm steps are suggestive of a stepwise helical winding of the DNA around the filamentous core of the viruslike particle during its growth in the AFS experiment, illustrated in Figure 6C. If we assume that the characteristic contour length of 30 nm corresponds to a single helical winding, this would imply a radius of the helix of 4.5 nm, and a radius of curvature of 5.1 nm, to arrive at a distance between the helical windings of 10 nm, consistent with the observed packing parameter of 3 (Fig. S8). This helical arrangement is large enough for the DNA to wind around the filamentous core of the VLP yet small enough to be within the region into which the binding blocks can extend. Interestingly, a DNA molecule wrapped around histones has a similar radius of curvature.[46]

To summarize, we have presented a unique combination of complementary, dynamic techniques for assembly studies of both VLPs and naturally evolved virus particles. We have used these techniques to address key issues regarding capsid assembly pathways that are difficult to address other than with real-time, single-particle methods: the nature of the critical nuclei for productive capsid formation and the dynamics and nature of nucleic acid condensation during capsid formation. Albeit our study focuses on nucleocapsid formation by simple artificial polypeptides, it does pave the way for the detailed real-time *in vitro* studies of the assembly of naturally evolved viruses at the single-particle level.

Methods. *Viruslike Particle Capsid Polypeptides.* The polypeptide, C−S_{10}−B, consists of three blocks that each encode a specific physicochemical functionality, mimicking corresponding functionalities of viral capsid proteins. Nucleic acid binding is achieved through interactions with block B that consists of 12 positively charged lysines. The silklike middle blocks S_{10} = $(GAGAGAGQ)_{10}$ fold into a sheetlike beta-solenoid conformation[35,47] (Figure 1A), and stacking of these sheets leads to the formation of a rigid protein filament that forms the core of the VLP.[20] Folding of an initially unfolded silk block into the beta-solenoid conformation is promoted by docking onto an already existing folded silk block, such that the formation of the rod-shaped protein core is a nucleated process.[20,21,35] Finally, a hydrophilic random-coil C, with a collagen-like sequence C = $(GXY)_{132}$ (where X and Y are mostly hydrophilic uncharged amino acids[48]) provides colloidal stability to the rod-shaped VLPs. Immediately after dissolution, the silk blocks of C−S_{10}−B polypeptides are still unfolded, but over time they fold and stack, a process that is strongly promoted by binding to the nucleic acid templates, such that coassembly with nucleic acid templates is favored over capsid protein-only assembly.[20] The biosyntethic capsid polypeptides were provided as lyophilized protein polymer powder (C−S_{10}−B = 44.7492 kDa), produced as previously described.[20] For additional sample preparation details, see the Supporting Information.

Atomic Force Microscopy. Viruslike particles were imaged in peak force tapping mode on a Bruker Bioscope catalyst setup, unless otherwise stated. Peptides and DNA were incubated with a final charge ratio N/P = 3 (molar ratio between positively charged NH_2 groups from the binding block to negatively charged PO_3 groups of the DNA template (P)), in 10 mM phosphate buffer at pH 7.5. Viruslike particles were adhered to freshly cleaved mica treated with 5 mM TRIS and 0.5 mM Mg^{2+} solution. For additional info on sample preparation for experiments in air and in liquid, see the Supporting Information. AFM image processing was performed with NanoScope Analysis 1.5 software for both a first order imaging flattening and the particles height estimation.

Optical Tweezers with Confocal Fluorescence Microscopy. The dual-trap optical tweezers setup with integrated

DOI: 10.1021/acs.nanolett.9b02376
Nano Lett. 2019, 19, 5746−5753

confocal fluorescence microscopy (LUMICKS) is similar to an optical setup used for dual-trap optical trapping experiments in combination with confocal fluorescence and a microfluidics flow-cell the has been described previously.[49] End-biotinylated bacteriophage λ DNA was connected to streptavidin-coated polystyrene beads (diameter = 4.5 μm, Spherotech) to generate the DNA constructs, as described previously.[50] For sample preparation and kymograph recording settings, see the Supporting Information. Binding of single peptides was followed through kymograph analysis quantifying their fluorescence signal (average number of photons) when landing on the DNA. All values were background corrected. We processed the kymographs through single-molecule tracking to acquire information on the binding events intensity and mobility. Photo bleaching allows one to calibrate the intensity of a single fluorophore (12.0 ± 0.5 photons) by looking at single fluorescence decrease steps of single photobleached dyes,[28,51−53] see Fig. S3. The one-dimensional diffusion of protein complexes along the DNA was quantified by tracking the peptides traces and calculating their diffusion coefficient (D) by using a mean square displacement analysis (MSD).[31] Force−distance curves and confocal fluorescence data were analyzed using a custom-written MATLAB software, using the extensible wormlike chain model (eWLC),[54] which describes the dsDNA elastic behavior up to ∼30 pN, is used to fit FDCs and estimate the DNA effective persistence length L_p:

$$x = L_c\left[1 - \frac{1}{2}\left(\frac{k_B T}{F L_p}\right)^{1/2} + \frac{F}{K}\right].$$

Acoustic Force Spectroscopy. The home-built AFS setup[32,55] and the AFS flow-cell (LUMICKS) and tethers preparation[55] have been previously described. The 8.4 kbp DNA was obtained from a pKYBI vector, as previously described.[55] For the preparation of functionalized DNA samples and flow-cell preparation, see the Supporting Information. AFS data were analyzed using a custom-written LABVIEW software, and the step-analysis was performed with a custom-made change-point analysis software.[33] Processed data were analyzed using Origin. In the Gaussian fit in Figure 5C, the peak-to-peak distances obtained are 22.6 ± 2, 21.3 ± 0.4, and 21 ± 0.3 nm for the histograms from top to bottom. The light blue backgrounds highlight the mean of the first two Gaussian peaks. In the main text, these values are corrected for the force applied during the experiments and the observed change in the effective L_p, resulting in an average step of 30 nm.

Electrophoretic Mobility Shift Assay (EMSA). EMSAs were performed to determine the effect of the dsDNA length on the protein binding. For sample preparation details, see the Supporting Information. The samples were loaded on 20% acrylamide gels in 1× TAE buffer and run at 70 V for 90 min. Gels were in a gel documentation system and analyzed with ImageJ. the N/P ratio for 50% binding of DNA (K_{Dapp}) by the protein was calculated fitting the DNA free intensities to the Hill equation, fraction bound $= \frac{1}{1 + \left(\frac{K_{Dapp}}{[C_4S_{0-10}B]}\right)^n}$, with n as the Hill constant.

■ ASSOCIATED CONTENT

Supporting Information

The Supporting Information is available free of charge on the ACS Publications website at DOI: 10.1021/acs.nanolett.9b02376.

Detailed information on VLP polypeptides, on AFM, optical tweezers with confocal fluorescence, AFS and EMSA methods; AFM, optical tweezers, confocal fluorescence, EMSA and AFS images, and data graphs; models of DNA compaction and DNA helix dimensions; and description of Langmuir dynamics (PDF)

■ AUTHOR INFORMATION

Corresponding Authors

*E-mail: w.h.roos@rug.nl .
*E-mail: gwuite@nat.vu.nl.

ORCID

Renko de Vries: 0000-0001-8664-3135
Wouter H. Roos: 0000-0002-5104-0139

Author Contributions

×G.J.L.W. and W.H.R. contributed equally

Notes

The authors declare the following competing financial interest(s): The optical tweezers-fluorescence and Acoustic Force Spectroscopy technology used in this study is patented and licensed to LUMICKS B.V., in which G.J.L.W. has a financial interest.

■ ACKNOWLEDGMENTS

This work was supported by a STW HTSM grant (to G.J.L.W. and W.H.R.) and a NWO Vidi grant (to W.H.R.). We thank Daan Vorselen for providing the steps-finding algorithm, Denise Denning for performing the AFM measurements in liquid, and Andreas Biebricher for support with the AFM experiments.

■ REFERENCES

(1) Katen, S.; Zlotnick, A. The thermodynamics of virus capsid assembly. *Methods Enzymol.* **2009**, *455*, 395−417.
(2) Mah, C.; Byrne, B. J.; Flotte, T. R. Virus-Based Gene Delivery Systems. *Clin. Pharmacokinet.* **2002**, *41* (12), 901−911.
(3) Rohovie, M. J.; Nagasawa, M.; Swartz, J. R. Virus-like particles: Next-generation nanoparticles for targeted therapeutic delivery. *Bioeng Transl Med.* **2017**, *2* (1), 43−57.
(4) Yang, N. An overview of viral and nonviral delivery systems for microRNA. *Int. J. Pharm. Investig* **2015**, *5* (4), 179−81.
(5) Selzer, L.; Katen, S. P.; Zlotnick, A. The Hepatitis B Virus Core Protein Intradimer Interface Modulates Capsid Assembly and Stability. *Biochemistry* **2014**, *53* (34), 5496−5504.
(6) Chevreuil, M.; et al. Nonequilibrium self-assembly dynamics of icosahedral viral capsids packaging genome or polyelectrolyte. *Nat. Commun.* **2018**, *9* (1), 3071.
(7) Prevelige, P. E.; Thomas, D.; King, J. Nucleation and growth phases in the polymerization of coat and scaffolding subunits into icosahedral procapsid shells. *Biophys. J.* **1993**, *64* (3), 824−35.
(8) Uetrecht, C.; Barbu, I. M.; Shoemaker, G. K.; van Duijn, E.; Heck, A. J. R. Interrogating viral capsid assembly with ion mobility−mass spectrometry. *Nat. Chem.* **2011**, *3* (2), 126−132.
(9) Kraft, D. J.; Kegel, W. K.; van der Schoot, P. A Kinetic Zipper Model and the Assembly of Tobacco Mosaic Virus. *Biophys. J.* **2012**, *102* (12), 2845−2855.
(10) Li, S.; Orland, H.; Zandi, R. Self consistent field theory of virus assembly. *J. Phys.: Condens. Matter* **2018**, *30* (14), 144002.

DOI: 10.1021/acs.nanolett.9b02376
Nano Lett. 2019, 19, 5746−5753

(11) Perlmutter, J. D.; Qiao, C.; Hagan, M. F. Viral genome structures are optimal for capsid assembly. *eLife* **2013**, *2*, No. e00632.
(12) Roos, W. H.; Bruinsma, R.; Wuite, G. J. L. Physical virology. *Nat. Phys.* **2010**, *6* (10), 733−743.
(13) Casini, G. L.; Graham, D.; Heine, D.; Garcea, R. L.; Wu, D. T. In vitro papillomavirus capsid assembly analyzed by light scattering. *Virology* **2004**, *325* (2), 320−327.
(14) Hagan, M. F.; Elrad, O. M. Understanding the Concentration Dependence of Viral Capsid Assembly Kinetics—the Origin of the Lag Time and Identifying the Critical Nucleus Size. *Biophys. J.* **2010**, *98* (6), 1065−1074.
(15) Garmann, R. F.; Comas-Garcia, M.; Knobler, C. M.; Gelbart, W. M. Physical Principles in the Self-Assembly of a Simple Spherical Virus. *Acc. Chem. Res.* **2016**, *49* (1), 48−55.
(16) Doerschuk, P. C.; Gong, Y.; Xu, N.; Domitrovic, T.; Johnson, J. E. Virus particle dynamics derived from CryoEM studies. *Curr. Opin. Virol.* **2016**, *18*, 57−63.
(17) Baclayon, M.; Wuite, G. J. L.; Roos, W. H. Imaging and manipulation of single viruses by atomic force microscopy. *Soft Matter* **2010**, *6* (21), 5273.
(18) Medrano, M.; et al. Imaging and Quantitation of a Succession of Transient Intermediates Reveal the Reversible Self-Assembly Pathway of a Simple Icosahedral Virus Capsid. *J. Am. Chem. Soc.* **2016**, *138* (47), 15385−15396.
(19) Zhou, J.; et al. Characterization of Virus Capsids and Their Assembly Intermediates by Multicycle Resistive-Pulse Sensing with Four Pores in Series. *Anal. Chem.* **2018**, *90* (12), 7267−7274.
(20) Hernandez-Garcia, A.; et al. Design and self-assembly of simple coat proteins for artificial viruses. *Nat. Nanotechnol.* **2014**, *9* (9), 698−702.
(21) Punter, M. T. J. J. M.; Hernandez-Garcia, A.; Kraft, D. J.; de Vries, R.; van der Schoot, P. Self-Assembly Dynamics of Linear Virus-Like Particles: Theory and Experiment. *J. Phys. Chem. B* **2016**, *120* (26), 6286−6297.
(22) Heller, I.; Hoekstra, T. P.; King, G. A.; Peterman, E. J. G.; Wuite, G. J. L. Optical Tweezers Analysis of DNA−Protein Complexes. *Chem. Rev.* **2014**, *114* (6), 3087−3119.
(23) Hashemi Shabestari, M.; Meijering, A. E. C.; Roos, W. H.; Wuite, G. J. L.; Peterman, E. J. G. Recent Advances in Biological Single-Molecule Applications of Optical Tweezers and Fluorescence Microscopy. *Methods Enzymol.* **2017**, *582*, 85−119.
(24) Chaurasiya, K. R.; Paramanathan, T.; McCauley, M. J.; Williams, M. C. Biophysical characterization of DNA binding from single molecule force measurements. *Phys. Life Rev.* **2010**, *7* (3), 299−341.
(25) Popov, Y. O.; Tkachenko, A. V. Effects of kinks on DNA elasticity. *Phys. Rev. E* **2005**, *71* (5), 51905.
(26) Lee, N.-K.; et al. Elasticity of Cisplatin-Bound DNA Reveals the Degree of Cisplatin Binding. *Phys. Rev. Lett.* **2008**, *101* (24), 248101.
(27) Hernandez-Garcia, A.; Werten, M. W. T.; Stuart, M. C.; de Wolf, F. A.; de Vries, R. Coating of Single DNA Molecules by Genetically Engineered Protein Diblock Copolymers. *Small* **2012**, *8* (22), 3491−3501.
(28) Brouwer, I.; et al. Sliding sleeves of XRCC4−XLF bridge DNA and connect fragments of broken DNA. *Nature* **2016**, *535* (7613), 566−569.
(29) Plazinski, W.; Rudzinski, W.; Plazinska, A. Theoretical models of sorption kinetics including a surface reaction mechanism: A review. *Adv. Colloid Interface Sci.* **2009**, *152* (1−2), 2−13.
(30) Zandi, R.; van der Schoot, P.; Reguera, D.; Kegel, W.; Reiss, H. Classical Nucleation Theory of Virus Capsids. *Biophys. J.* **2006**, *90* (6), 1939−1948.
(31) Heller, I.; et al. Mobility Analysis of Super-Resolved Proteins on Optically Stretched DNA: Comparing Imaging Techniques and Parameters. *ChemPhysChem* **2014**, *15* (4), 727−733.
(32) Sitters, G.; et al. Acoustic force spectroscopy. *Nat. Methods* **2015**, *12* (1), 47−50.
(33) Yang, H. Change-Point Localization and Wavelet Spectral Analysis of Single-Molecule Time Series. In *Single-Molecule Biophysics*; Advances in Chemical Physics, Vol. *146*; John Wiley & Sons, Inc.: Hoboken, NJ, 2011; pp 217−243,
(34) Zandi, R.; van der Schoot, P.; Reguera, D.; Kegel, W.; Reiss, H. Classical Nucleation Theory of Virus Capsids. *Biophys. J.* **2006**, *90* (6), 1939−1948.
(35) Cingil, H. E.; et al. Illuminating the Reaction Pathways of Viromimetic Assembly. *J. Am. Chem. Soc.* **2017**, *139* (13), 4962−4968.
(36) Hu, T.; Shklovskii, B. I. Kinetics of viral self-assembly: role of the single-stranded RNA antenna. *Phys. Rev E Stat. Nonlin. Soft Matter Phys.* **2007**, *75*, 051901.
(37) Kivenson, A.; Hagan, M. F. Mechanisms of Capsid Assembly around a Polymer. *Biophys. J.* **2010**, *99* (2), 619−628.
(38) Zhao, B.; Cohen Stuart, M. A.; Hall, C. K. Navigating in foldonia: Using accelerated molecular dynamics to explore stability, unfolding and self-healing of the β-solenoid structure formed by a silk-like polypeptide. *PLoS Comput. Biol.* **2017**, *13* (3), No. e1005446.
(39) Razzokov, J.; Naderi, S.; van der Schoot, P. Nanoscale insight into silk-like protein self-assembly: effect of design and number of repeat units. *Phys. Biol.* **2018**, *15* (6), 066010.
(40) Odijk, T. Statics and dynamics of condensed DNA within phages and globules. *Philos. Trans. R. Soc., A* **2004**, *362* (1820), 1497−517.
(41) Leforestier, A.; Livolant, F. Structure of toroidal DNA collapsed inside the phage capsid. *Proc. Natl. Acad. Sci. U. S. A.* **2009**, *106* (23), 9157−62.
(42) Petrov, A. S.; Harvey, S. C. Packaging Double-Helical DNA into Viral Capsids: Structures, Forces, and Energetics. *Biophys. J.* **2008**, *95* (2), 497−502.
(43) Eber, F. J.; Eiben, S.; Jeske, H.; Wege, C. RNA-controlled assembly of tobacco mosaic virus-derived complex structures: from nanoboomerangs to tetrapods. *Nanoscale* **2015**, *7* (1), 344−355.
(44) Fritsche, M.; Heermann, D. W. Confinement driven spatial organization of semiflexible ring polymers: Implications for biopolymer packaging. *Soft Matter* **2011**, *7* (15), 6906.
(45) Odijk, T. Scaling theory of DNA confined in nanochannels and nanoslits. *Phys. Rev. E* **2008**, *77* (6), 60901.
(46) Richmond, T. J.; Davey, C. A. The structure of DNA in the nucleosome core. *Nature* **2003**, *423* (6936), 145−150.
(47) Zhao, B.; Cohen Stuart, M. A.; Hall, C. K. Dock 'n roll: folding of a silk-inspired polypeptide into an amyloid-like beta solenoid. *Soft Matter* **2016**, *12* (16), 3721−3729.
(48) Werten, M. W. T.; Wisselink, W. H.; Jansen-van den Bosch, T. J.; de Bruin, E. C.; de Wolf, F. A. Secreted production of a custom-designed, highly hydrophilic gelatin in Pichia pastoris. *Protein Eng., Des. Sel.* **2001**, *14* (6), 447−454.
(49) Heller, I.; et al. STED nanoscopy combined with optical tweezers reveals protein dynamics on densely covered DNA. *Nat. Methods* **2013**, *10* (9), 910−6.
(50) Gross, P.; Farge, G.; Peterman, E. J. G.; Wuite, G. J. L. Combining Optical Tweezers, Single-Molecule Fluorescence Microscopy, and Microfluidics for Studies of DNA−Protein Interactions. *Methods Enzymol.* **2010**, *475*, 427−453.
(51) Noom, M. C.; van den Broek, B.; van Mameren, J.; Wuite, G. J. L. Visualizing single DNA-bound proteins using DNA as a scanning probe. *Nat. Methods* **2007**, *4* (12), 1031−1036.
(52) Candelli, A.; et al. Visualization and quantification of nascent RAD51 filament formation at single-monomer resolution. *Proc. Natl. Acad. Sci. U. S. A.* **2014**, *111* (42), 15090−5.
(53) King, G. A.; et al. Acetylation and phosphorylation of human TFAM regulate TFAM−DNA interactions via contrasting mechanisms. *Nucleic Acids Res.* **2018**, *46* (7), 3633−3642.
(54) Odijk, T. Stiff Chains and Filaments under Tension. *Macromolecules* **1995**, *28*, 7016−7018.
(55) Kamsma, D.; Wuite, G. J. L. Single-Molecule Measurements Using Acoustic Force Spectroscopy (AFS). In *Single Molecule Analysis*; Methods in Molecular Biology, Vol. *1665*; Springer New York: New York, 2018; pp 341−351,

DOI: 10.1021/acs.nanolett.9b02376
Nano Lett. 2019, 19, 5746−5753